GEOPHYSICS. VOL. 76, NO. 5 (SEPTEMBER-OCTOBER 2011); P. R135–R146, 11 FIGS., 1 TABLE.
10.1190/GEO2010-0159.1

Least-squares migration of multisource data with a deblurring filter

Wei Dai[1], Xin Wang[1], and Gerard T. Schuster[2]

ABSTRACT

Least-squares migration (LSM) has been shown to be able to produce high-quality migration images, but its computational cost is considered to be too high for practical imaging. We have developed a multisource least-squares migration algorithm (MLSM) to increase the computational efficiency by using the blended sources processing technique. To expedite convergence, a multisource deblurring filter is used as a preconditioner to reduce the data residual. This MLSM algorithm is applicable with Kirchhoff migration, wave-equation migration, or reverse time migration, and the gain in computational efficiency depends on the choice of migration method. Numerical results with Kirchhoff LSM on the 2D SEG/EAGE salt model show that an accurate image is obtained by migrating a supergather of 320 phase-encoded shots. When the encoding functions are the same for every iteration, the input/output cost of MLSM is reduced by 320 times. Empirical results show that the crosstalk noise introduced by blended sources is more effectively reduced when the encoding functions are changed at every iteration. The analysis of signal-to-noise ratio (S/N) suggests that not too many iterations are needed to enhance the S/N to an acceptable level. Therefore, when implemented with wave-equation migration or reverse time migration methods, the MLSM algorithm can be more efficient than the conventional migration method.

INTRODUCTION

Conventional migration (Claerbout, 1971) computes the reflectivity image by applying the adjoint operator to the data. Migration can also be interpreted as the first iteration of iterative inversion, in which the Hessian of the misfit functional is approximated as a diagonal matrix. This approximation is violated when the data are incomplete (Nemeth et al., 1999) and the migration image will be obscured by migration artifacts.

It has been shown that least-squares migration (LSM) (Nemeth et al., 1999; Duquet et al., 2000) can improve the resolution of the migration image and suppress migration artifacts. However, one of the drawbacks of LSM is its high computational cost. In this paper, we propose to use a summation of phase-encoded shot gathers as input data to reduce the computational burden of LSM. The blended data are similar to that used in the blended sources method (Romero et al., 2000), but our proposed scheme of multisource least-squares migration (MLSM) aims to improve the image quality while reducing crosstalk noise. During the inversion, a deblurring filter is used as a preconditioner (Hu and Schuster, 2000; Guitton, 2004; Aoki and Schuster, 2009) to speed up the convergence.

Blended sources processing

In blended sources processing, many conventionally acquired shot gathers are phase-encoded and blended together to form supergathers to reduce the computational cost and input/output (I/O) burden of migration. Romero et al. (2000) first explored this idea with the wave-equation migration of synthetic data associated with the Marmousi model. They produced acceptable images with less cost than the conventional method. The limitation of their approach was that the blended sources images were always no better in quality than the corresponding conventional images because the blended sources introduced unacceptable crosstalk noise into the final migration section. To increase the computational efficiency of full waveform inversion, Zhan et al. (2011) apply the multisource multiscale waveform inversion to 2D synthetic data and used a deblurring filter to reduce the crosstalk error. Their numerical results showed a 12-fold speedup in computation efficiency. Krebs et al. (2009) present their full waveform inversion result with blended sources encoded by random encoding functions. Their computational efficiency was increased by a factor of 50 compared

Manuscript received by the Editor 22 May 2010; revised manuscript received 1 May 2011; published online 22 November 2011.
[1]University of Utah, Department of Geology and Geophysics, Salt Lake City, Utah, USA; King Abdullah University of Science and Technology, Physical Science and Engineering Division, Thuwal, Saudi Arabia. E-mail: wei.dai@utah.edu; xin.wang@utah.edu.
[2]King Abdullah University of Science and Technology, Physical Science and Engineering Division, Thuwal, Saudi Arabia. E-mail: gerard.schuster@kaust.edu.sa.

with standard full waveform inversion, and their method has been mostly tested for a fixed-spread acquisition geometry. The extension of blended sources processing to marine acquisition is a topic of current research.

Crosstalk noise reduction

As mentioned earlier, blended sources processing introduces crosstalk noise, which needs to be removed from the final migration images. Simultaneous sources acquisition shares some common ground with blended sources, as it reduces the acquisition cost, but introduces crosstalk noise also. The simplest approach for reducing crosstalk noise in multisource data is to use standard migration and stacking procedures. Lynn et al. (1987) show that coherent noise in multisource data (with several shot gathers per supergather) can effectively be suppressed by weighted stacking. Hampson et al. (2008) report their synthetic and field data examples and show that for 2D cases and two shot gathers per supergather, simple stacking was effective enough, but for their 3D example, they found that the shot separation technique was necessary due to the strong reflections from the shallow-water bottom. Fromyr et al. (2008) achieve similar image quality with two-source shooting as compared with conventional acquisition in their wide azimuth experiment. With careful survey design, a suitable marine environment and a small number of multiple sources, simple stacking alone might be sufficient for quality imaging. To assist in this design process, Schuster et al. (2011) provide rigorous formulas for predicting the level of crosstalk noise as a function of the encoding parameters.

Scope of this paper

In this paper, an MLSM algorithm is proposed to combine the strengths of LSM and blended sources processing to produce high quality images with low computational cost. The LSM improves the image quality by suppressing migration artifacts, balancing reflector amplitudes and enhancing image resolution, and blended sources processing increases the computational efficiency. During the iterations of LSM, the crosstalk noise introduced by blended sources is effectively reduced. The MLSM algorithm can be implemented with any migration method and the gain in efficiency depends on the migration method. Our goal is to test the effectiveness of the MLSM algorithm with a Kirchhoff migration method.

This paper is organized into the following three sections. The first part presents the theory of phase-encoded LSM of supergathers. The next section presents synthetic results that demonstrate the efficiency and effectiveness of the MLSM algorithm. Finally, a summary is provided.

THEORY

For a fixed-spread acquisition, the phase-encoded multisource data (i.e., supergathers) can be represented as

$$\mathbf{d} = \sum_{i=1}^{S} \mathbf{P}_i \mathbf{d}_i, \tag{1}$$

where S is the number of multiple shots and matrix $\mathbf{P}_i$ represents the phase-encoding functions (in this study, the encoding functions involve random source time delay). All the $\mathbf{P}_i$ are chosen to be unitary so that $\mathbf{P}_i^T \mathbf{P}_i$ is equal to the identity matrix.

In equation 1, we define $\mathbf{d}$ as a supergather, which is the summation of shot gathers, each with shot excitation time shifted by a random time shift with a standard deviation greater than the source period. It is shown in Schuster et al. (2011) that the combination of random polarity changes, random time shifts and random shot locations is more effective at reducing crosstalk noise than the use of any of the three encoding functions alone. We assume that the ith CSG $\mathbf{d}_i$ and the reflectivity model $\mathbf{m}$ are related by

$$\mathbf{d}_i = \mathbf{L}_i \mathbf{m}, \tag{2}$$

where $\mathbf{L}_i$ is the linear forward modeling operator associated with the ith shot. This operator can represent either a Kirchhoff or a wave-equation modeling method (Mulder and Plessix, 2004). Plugging equation 2 into 1, we get

$$\mathbf{d} = \sum_{i=1}^{S} \mathbf{P}_i \mathbf{L}_i \mathbf{m} = \mathbf{L}\mathbf{m}, \tag{3}$$

where the supergather modeling operator is defined as

$$\mathbf{L} = \sum_{i=1}^{S} \mathbf{P}_i \mathbf{L}_i. \tag{4}$$

Multisource migration

From equation 4, the supergather migration operator is defined as the adjoint of the supergather modeling operator,

$$\mathbf{L}^T = \sum_{i=1}^{S} \mathbf{L}_i^T \mathbf{P}_i^T, \tag{5}$$

so that the supergather migration image is

$$\begin{aligned}
\mathbf{m}_{\text{mig}} &= \mathbf{L}^T \mathbf{d} = \mathbf{L}^T \sum_{i=1}^{S} \mathbf{P}_i \mathbf{L}_i \mathbf{m} \\
&= \sum_{j=1}^{S} \mathbf{L}_j^T \mathbf{P}_j^T \sum_{i=1}^{S} \mathbf{P}_i \mathbf{L}_i \mathbf{m} \\
&= \sum_{i=1}^{S} \sum_{j=1}^{S} \mathbf{L}_j^T \mathbf{P}_j^T \mathbf{P}_i \mathbf{L}_i \mathbf{m} \\
&= \overbrace{\sum_{i=1}^{S} \mathbf{L}_i^T \mathbf{L}_i \mathbf{m}}^{\text{standard migration image}} + \overbrace{\sum_{j \neq i} \sum_{i=1}^{S} \mathbf{L}_j^T \mathbf{P}_j^T \mathbf{P}_i \mathbf{L}_i \mathbf{m}}^{\text{crosstalk}},
\end{aligned} \tag{6}$$

consisting of two terms: the first term is the standard migration image, and the second term is the crosstalk noise introduced by multisource blending of shot gathers. The magnitude of the crosstalk term for a variety of different phase-encoding functions is derived in Schuster et al. (2011).

Multisource least-squares migration (MLSM)

To suppress crosstalk noise to an acceptable level when the number of multiple sources S is large, we solve equation 3 in the least-squares sense (Dai and Schuster, 2009; Dai et al., 2009). That is, define the objective function as

$$f(\mathbf{m}) = \frac{1}{2}\|\mathbf{d} - \mathbf{Lm}\|^2 + \frac{1}{2}\lambda\|\mathbf{m} - \mathbf{m}_{\text{apr}}\|^2, \qquad (7)$$

so that, an optimal $\mathbf{m}$ is sought to minimize the objective function in equation 7. In equation 7, Tikhonov regularization (Tikhonov and Arsenin, 1977) is used, and λ is the regularization parameter that is determined by a trial and error method. Smoothness constraints in the form of second-order derivatives of the model function can expedite convergence (Kühl and Sacchi, 2003) and partly overcome the problems associated with errors in the velocity model.

With the assumption that nothing is known about $\mathbf{m}$, $\mathbf{m}_{\text{apr}}$ is set to be equal to zero. The model $\mathbf{m}$ that minimizes equation 7 can be found by a gradient type optimization method

$$\mathbf{m}^{(k+1)} = \mathbf{m}^{(k)} - \alpha\mathbf{F}(\mathbf{L}^T(\mathbf{Lm}^{(k)} - \mathbf{d}) + \lambda\mathbf{m}^{(k)}), \qquad (8)$$

where $\mathbf{L}^T(\mathbf{Lm}^{(k)} - \mathbf{d}) + \lambda\mathbf{m}^{(k)}$ is the gradient, $\mathbf{F}$ is a preconditioning matrix, and α is the step length. Because both the forward modeling and migration operators are linear and adjoint to each other, the analytical step length formula can be used. Alternatively, to improve the robustness of the MLSM algorithm, a quadratic line-search method is carried out with the current model and two trial models. In this study, we use the conjugate gradient (CG) method, which generally converges faster than the steepest decent method. Moreover, static encoding is used where the encoding functions are the same for every iteration to reduce the I/O cost. Boonyasiriwat and Schuster (2010) show that dynamic encoding (encoding functions are changed at every iteration) is more effective in 3D multisource full waveform inversion and so dynamic encoding results are presented as well. To ensure the convergence of MLSM, the migration velocity should be close to the true velocity model.

Numerical implementation

The numerical scheme in equation 8 is applicable to any migration method and its associated forward modeling (demigration) operator. Each type of migration method, e.g., Kirchhoff migration, one-way wave-equation migration or reverse time migration, can be implemented in the mode of LSM (Nemeth et al., 1999; Duquet et al., 2000; Kaplan et al., 2010; Dai and Schuster, 2010). When combined with blended sources processing, each specific implementation will bear different advantages. The computational cost of the one-way wave-equation migration or reverse-time migration method is reduced by S times when S sources are blended together. In addition, the I/O cost is reduced by S times with static encoding method. On the other hand, the computational cost of Kirchhoff migration is relatively low, but it cannot be further reduced with blended sources processing because the Kirchhoff migration operation of $\mathbf{L}_i^T\mathbf{P}_i^T$ in equation 5 must be applied separately to the supergather for $i = 1, 2, ..., S$. However, the I/O cost is reduced by inputting only a supergather so this will reduce the overall run time of Kirchhoff LSM.

In this paper, the MLSM algorithm is implemented with Kirchhoff migration and tested on synthetic blended sources data. To expedite convergence, a deblurring filter (see Appendix A) is used as a preconditioner (Hu and Schuster, 2000; Guitton, 2004; Aoki and Schuster, 2009) that can reduce the migration artifacts related to Kirchhoff migration (frowns and smiles) and compensate for the energy loss from geometric spreading, and therefore, speeds up the convergence. Numerical simulations are conducted to validate these statements.

Signal-to-noise ratio analysis

It is desirable to estimate the relationship between the S/N, defined in Appendix B) enhancement and the number of shot gathers (S) for iterative LSM of supergathers. Although it affords no simple analytical expression for the dependence of S/N on the number of iterations of LSM, we focus on how the S/N is reduced by iterative stacking (multiple migrations of all shots) of Romero et al. (2000), where all the shots in a survey are phase-encoded and blended together to form a supergather before migration (Figure 1). Here, we assume the data are noise free and the noise is defined to be the crosstalk noise only. In other words, in equation 6 the "standard migration image" term is assumed to be noise free, whereas the "crosstalk" term is responsible for all the noise. For convenience, the terms in equation 6 are regrouped here as follows,

$$\mathbf{m}_{\text{mig}} = \sum_{i=1}^{S}\mathbf{m}_{\text{mig},i} = \sum_{i=1}^{S}\left(\overbrace{\mathbf{L}_i^T\mathbf{L}_i\mathbf{m}}^{\text{signal}} + \overbrace{\sum_{j\neq i}\mathbf{L}_j^T\mathbf{P}_j^T\mathbf{P}_i\mathbf{L}_i\mathbf{m}}^{\text{noise}}\right). \qquad (9)$$

In equation 9, we further assume the signal term and $S-1$ noise terms in the parentheses are of comparable energy, and that those $S-1$ noise terms are incoherent. Consequently, the S/N is roughly $1/\sqrt{S-1}$ for $\mathbf{m}_{\text{mig},i}$, the image associated with ith sources. After summation over all the S sources, the S/N of $\mathbf{m}_{\text{mig}}$ is $\sqrt{S}/\sqrt{S-1}$, assuming the signal term from all the S sources are coherent.

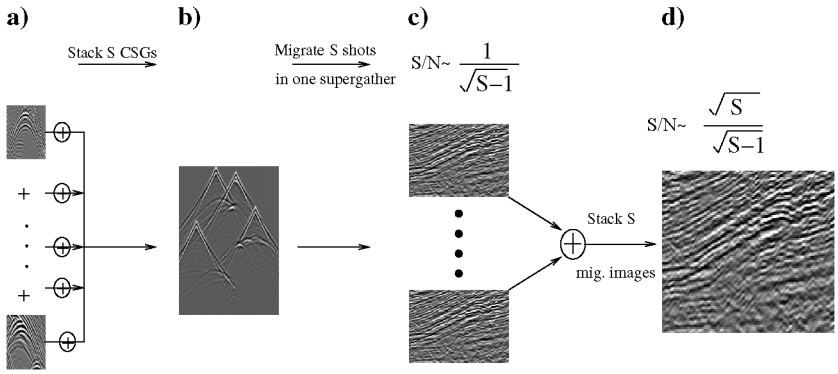

Figure 1. (a) Time-shifted shot gathers, (b) blended supergather created by blending S time-shifted shot gathers, (c) migration images after migrating the supergather for each shot position with S/N approximately $1/\sqrt{S-1}$, (d) final image after summing S migration images. The final S/N is $\sqrt{S}/\sqrt{S-1}$.

This S/N analysis is summarized in Figure 1. Here, S shots in Figure 1a are encoded and stacked together to form a supergather that is noise free, in Figure 1b. The supergather is then migrated S times — once for each of the S source locations — to produce S images, as shown in Figure 1c. Every image contains one signal image from a correctly decoded and migrated shot and $S-1$ noisy images from the rest $S-1$ shots being migrated with wrong source locations and wrong time shifts. As analyzed before, every image in Figure 1c has a S/N approximately $1/\sqrt{S-1}$. After stacking all the S images together in Figure 1d, the S/N becomes $\sqrt{S}/\sqrt{S-1}$. Here, the key assumptions are

- The correctly decoded and migrated shots from all the S images give coherent signal that will constructively stack after stacking. In addition, geometrical spreading effects can be ignored.
- The incorrectly decoded and migrated shots generate random noise with the same strength due to random encoding that will destructively stack after stacking.
- The crosstalk noise from each migration at each iteration is uncorrelated:

$$\mathrm{S/N} \approx \sqrt{SI}/\sqrt{S-1}. \tag{10}$$

In the case that there are N supergathers in the survey, the S/N is proportional to

$$\begin{aligned}\mathrm{S/N} &\approx \sqrt{NSI}/\sqrt{S-1} \\ &\approx \sqrt{NI}, \quad \text{when } S \gg 1,\end{aligned} \tag{11}$$

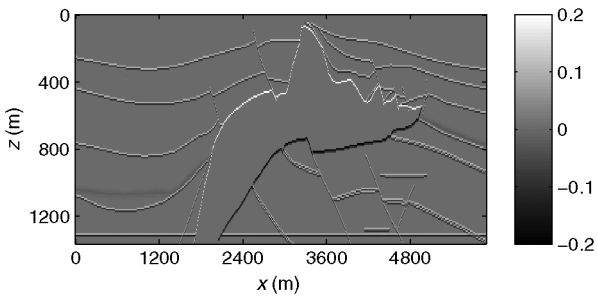

Figure 2. 2D SEG/EAGE salt model (reflectivity).

Table 1. Modeling parameters for conventional sources simulation.

Model size	645 × 150	Src wavelet	Ricker
Grid interval	9.14 m	Peak freq.	50 Hz
Src number	320	Src interval	18.3 m
Rec. number	320	Rec. interval	18.3 m
Trace length	4 s	Regularization	1.0e − 7
Subsec. size	5 × 5 pts	Filter size	3 × 3 pts

where N is the number of supergathers and I is the number of iterations. The total number of shots is $N \times S$. When S is equal to one for the conventional sources situation, there will be no crosstalk noise. Because we assume there is no noise in the original shot gathers, the S/N of the migration image is infinity, and when S is much greater than one, the S/N is independent of S. Equations 10 and 11 will be validated with numerical examples for $S \gg 1$. In the case of iterative LSM, the crosstalk noise in the gradient or conjugate direction from each iteration is correlated with each other for static encoding; moreover, after being scaled with the step length, the variance of the crosstalk noise would be different for every iteration, where early iterations receive large weight. Therefore, we expect the S/N enhancement to be less than the prediction from equation 11, where crosstalk noise is assumed to be of comparable energy.

When S is small, e.g., $S = 2$, the S/N of a conventional Kirchhoff migration image is often large enough, because N is large in this case. Several studies (Beasley, 2008; Hampson et al., 2008; Berkhout, 2008; Fromyr et al., 2008) have shown that conventional stacking and migration of simultaneously acquired supergathers can effectively suppress the interference of reflections from different sources, i.e., crosstalk. However, if S is large, the crosstalk noise is intolerable due to the decrease of the number of supergathers N. In the next section, MLSM is applied to synthetic multishot supergathers to suppress the crosstalk and improve the S/N.

NUMERICAL TESTS

The MLSM algorithm wth Kirchhoff modeling and adjoint operators is tested on synthetic data generated by a Born modeling method for the 2D SEG/EAGE salt model. Figure 2 shows the reflectivity model calculated from the velocity model by using vertical rays and constant density assumptions; the true velocity model is used for migration. The ocean bottom reflector is muted to better illustrate the deep structure, and 320 sources and 320 receivers are deployed on the surface with the same sampling interval of 18.3 m. The modeling parameters are listed in Table 1 (see Appendix A for the meaning of deblurring filter parameters), where the deblurring filter is only applied at the first two iterations[3] to provide a good initial model for the inversion. The regularization parameter is chosen based on a trial-and-error method and is reduced by half after each iteration. Regularization is important for attenuating crosstalk noise and high-frequency noise associated with the deblurring filter.

Conventional sources least-squares migration and deblurring

Figure 3a shows the 2D prestack Kirchhoff migration image (color scale boosted to show deep structures) for a conventional acquisition geometry of 320 individual shots with 320 receivers per shot. To reduce the artifacts, a nonstationary preconditioner (also denoted as a deblurring filter in Aoki and Schuster (2009)) is applied to the Kirchhoff migration image to give the result shown in Figure 3b. It is referred to as the deblurred image.

Comparison of the deblurred image and nondeblurred images shows that the deblurred image has a more balanced reflectivity amplitude, which indicates that amplitude weakening due to geometric spreading is compensated. The migration artifacts are also suppressed in the deblurred image. However, the deblurring filter also

[3]The standard preconditioner (Nemeth et al., 1999; Plessix and Mulder, 2004) of inverse geometric spreading is used at every iteration.

introduces some high-frequency noise into the deblurred image because it only approximates the inverse Hessian (see Appendix A for details). In the end, the filter is effective for deblurring Kirchhoff migration images, but it comes with the price of adding high-frequency noise. A more effective deblurring filter (Yu et al., 2006) can be used but comes with added computation cost.

To summarize the overall effect of the deblurring filter, Figure 4 depicts the convergence curves for both standard (CG) and deblurred LSM (it is referred to as DCG). Here, the CG result after one iteration is equivalent to the Kirchhoff migration image, and the first iteration result of DCG represents the deblurred image. We can see that the deblurring filter reduces the data residual by 52%, in spite of the high-frequency noise it introduced. It is not used after a few iterations and allows the LSM to reduce the remaining noise.

Figure 3c shows the conventional sources LSM image after 30 CG iterations[4], which is almost identical to the original model. It demonstrates that LSM can sometimes produce images of higher quality and resolution compared to Kirchhoff migration (Nemeth et al., 1999), if the migration velocity is a somewhat accurate rendering of the actual smoothed velocity.

Multisource least-squares migration

To simulate multisource data, conventional sources data are encoded and blended together to form a small number of supergathers. The 320 shot gathers are separated into different clusters of supergathers, where each supergather in a cluster is formed by stacking a unique set of shot gathers together to form the following data sets: 32 10-shot supergathers, 16 20-shot supergathers, eight 40-shot supergathers, four 80-shot supergathers, two 160-shot supergathers, and one 320-shot supergather. Each shot gather has a random time shift applied to it with a standard deviation equal to about seven times the dominant period of the source wavelet. All the random time shifts are generated by a random number generator that honors a uniform probability distribution. Figure 5 shows the Kirchhoff migration images from all the experiments. Consistent with equation 11, these results show that decreasing the number of supergather leads to increasing levels of crosstalk.

To further validate equation 11, we adopt the iterative stacking approach (multiple migrations of all shots) in Romero et al. (2000), where all the 320 shots are encoded and blended together and migrated with different encoding functions for many iterations. The migration images from different iterations are then stacked together to improve the S/N. Numerically, we use the formula,

$$\mathrm{S/N} = \frac{\|\mathbf{m}_{\mathrm{ref}}\|}{\|\mathbf{m}^{(k)} - \mathbf{m}_{\mathrm{ref}}\|}, \tag{12}$$

for the S/N calculation, where $\mathbf{m}_{\mathrm{ref}}$ is the reference migration image for conventional sources (Figure 3a) and $\mathbf{m}^{(k)}$ is the stacked image after k iterations (k-fold). According to equation 11, the S/N is proportional to $\sqrt{I}$, I being the number of iterations. The numerical results in Figure 6 largely agree with the prediction in which the measured S/N is normalized by the S/N of the first iteration to compare with the $\sqrt{I}$ curve. Figure 7a shows the Kirchhoff

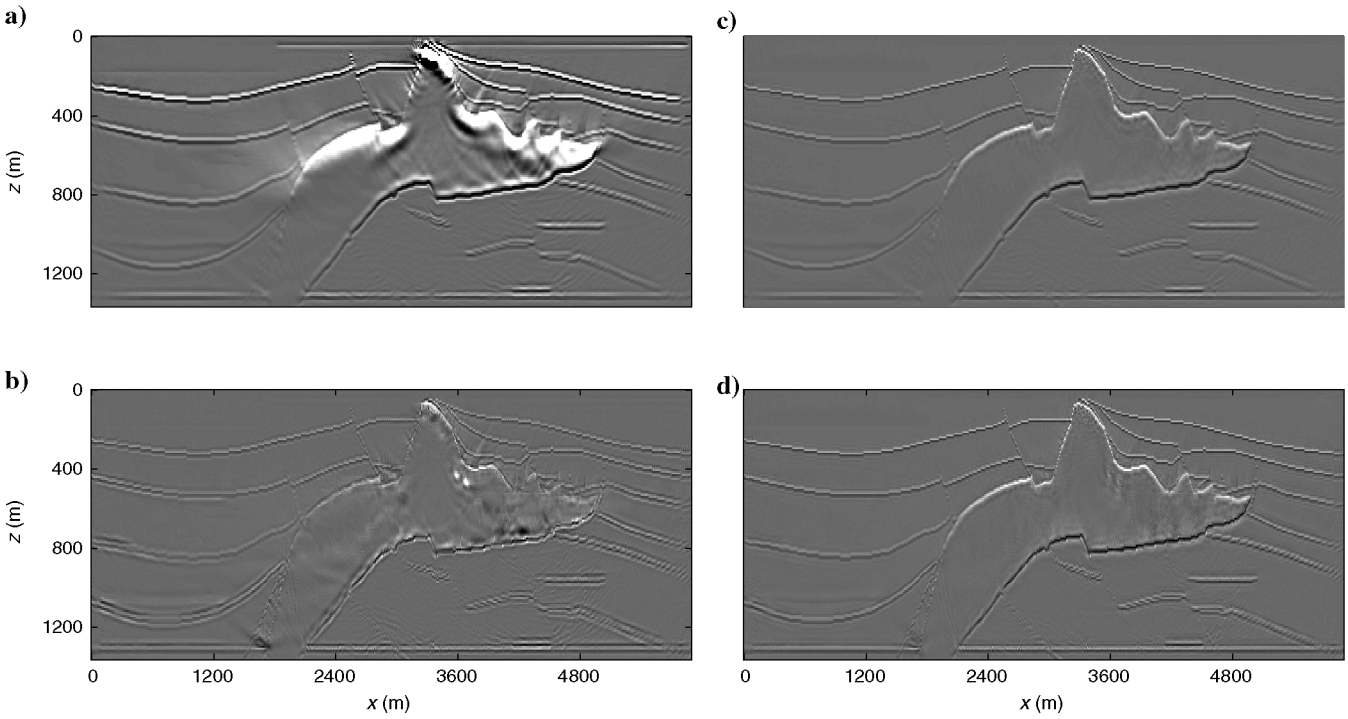

Figure 3. (a) Kirchhoff migration image for conventional sources data, (b) KM image after deblurring (deblurred image), (c) least-squares migration image after 30 CG iterations, (d) preconditioned LSM image after 30 DCG iterations.

[4]DCG produces basically the same result after so many iterations, shown in Figure 3d.

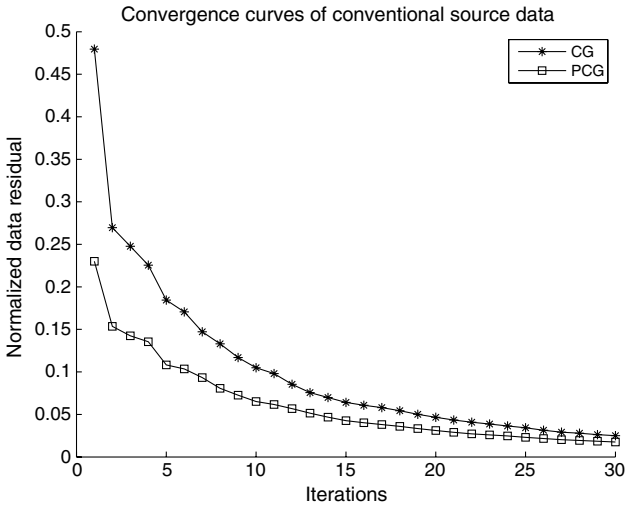

Figure 4. Normalized data residual plotted against iteration number. The line with stars indicates the convergence of the conjugate gradient method and the line with squares shows the convergence when the deblurring filter is used as a preconditioner.

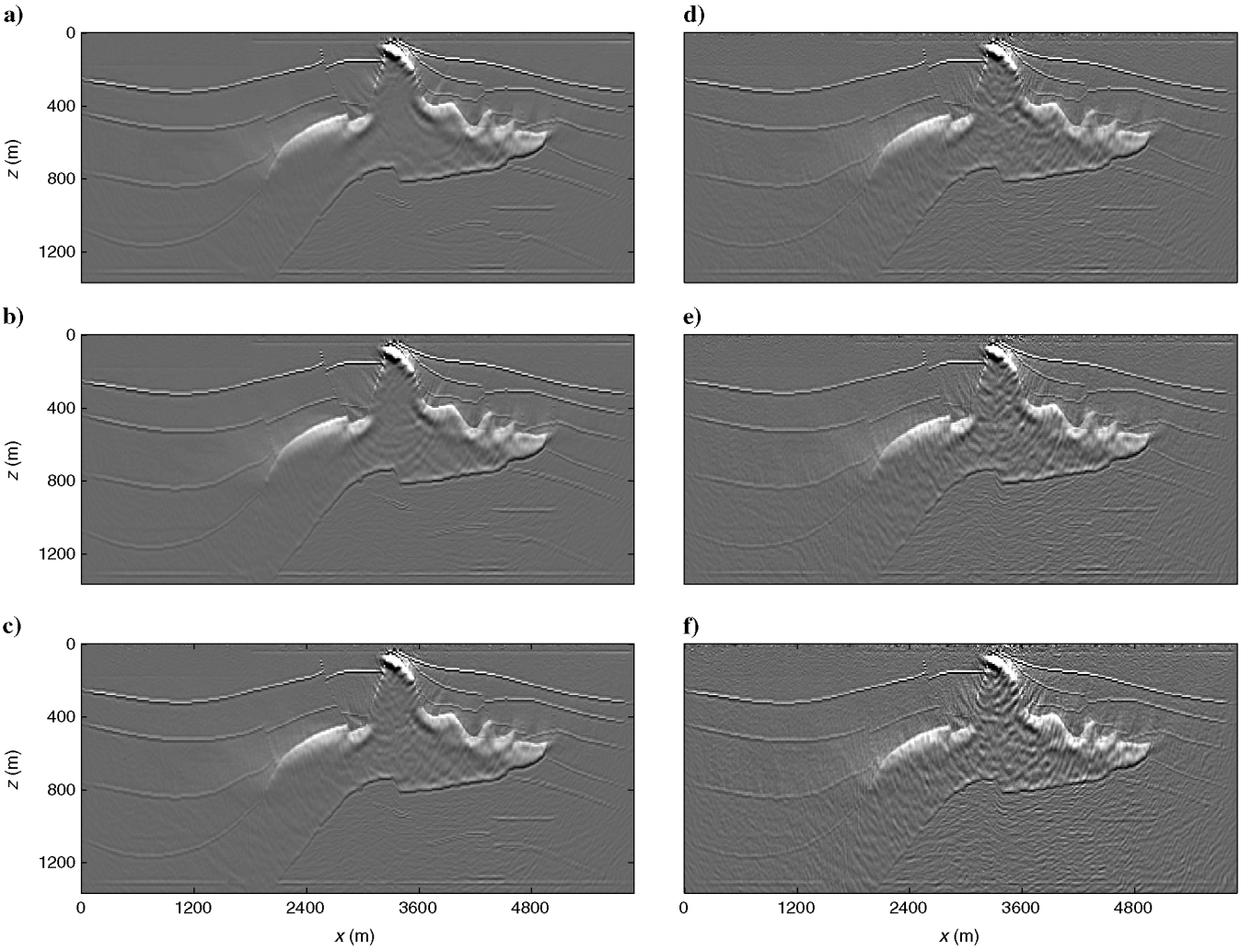

Figure 5. Kirchhoff migration images obtained from the following clusters of supergathers, (a) 32 10-shot supergathers, (b) 16 20-shot supergathers, (c) eight 40-shots supergathers, (d) four 80-shot supergathers, (e) two 160-shot supergathers, and (f) one 320-shot supergather. Here, all shot gathers consisted of 320 traces, and each supergather in a cluster was formed from a unique set of shot gathers.

migration image of a 320-shot supergather with only one stack ($I = 1$); Figure 7b the fivefold stacked image ($I = 5$); Figure 7c the 10-fold stacked image ($I = 10$); and Figure 7d the 20-fold stacked image ($I = 20$). These numerical results suggest that iterative stacking is very effective in suppressing random crosstalk noise. The iterative stacking method is applicable to marine data with either wave-equation or reverse-time migration, where the supergathers are not explicitly formed, but instead, the back-propagated wavefields are superimposed together. However, without LSM, these migration artifacts will persist in the images.

For the case where S is much greater than 1, Figure 8 presents the migration images in which the input data consist of only one supergather ($N = 1$, in equation 11) but there are different numbers of shot gathers in the supergather: Figure 8a $S = 40$, Figure 8b $S = 80$, and Figure 8c $S = 160$. These results, along with Figure 5f, demonstrate that the S/Ns of these migration images are mostly independent of the number of shot gathers in the supergather. At first glance, this result appears contradictory to intuition because the migration of a 160-shot supergather might be expected to yield a less noisy image than a 80-shot supergather. However, the 160-shot supergather has a higher crosstalk noise level (by a factor of $\sqrt{2}$) than the 80-shot supergather, which cancels the $\sqrt{2}$ S/N enhancement in migrating a 160-shot supergather. The key point here is that increasing the number of unique supergathers is more effective at S/N enhancement than increasing the number of unique shot gathers per supergather.

According to equation 11, even a single 320-shot supergather can be used to get an accurate image if the number of iterations is large

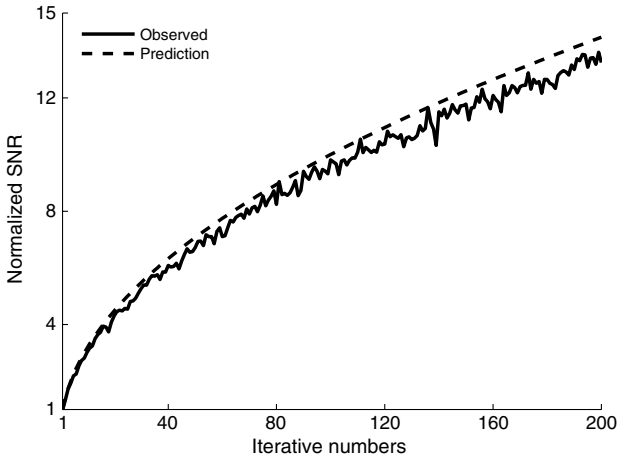

Figure 6. The predicted and measured S/N of iterative stacking method are plotted against iteration number as dashed and solid lines. The measurements have been normalized by the first iteration result.

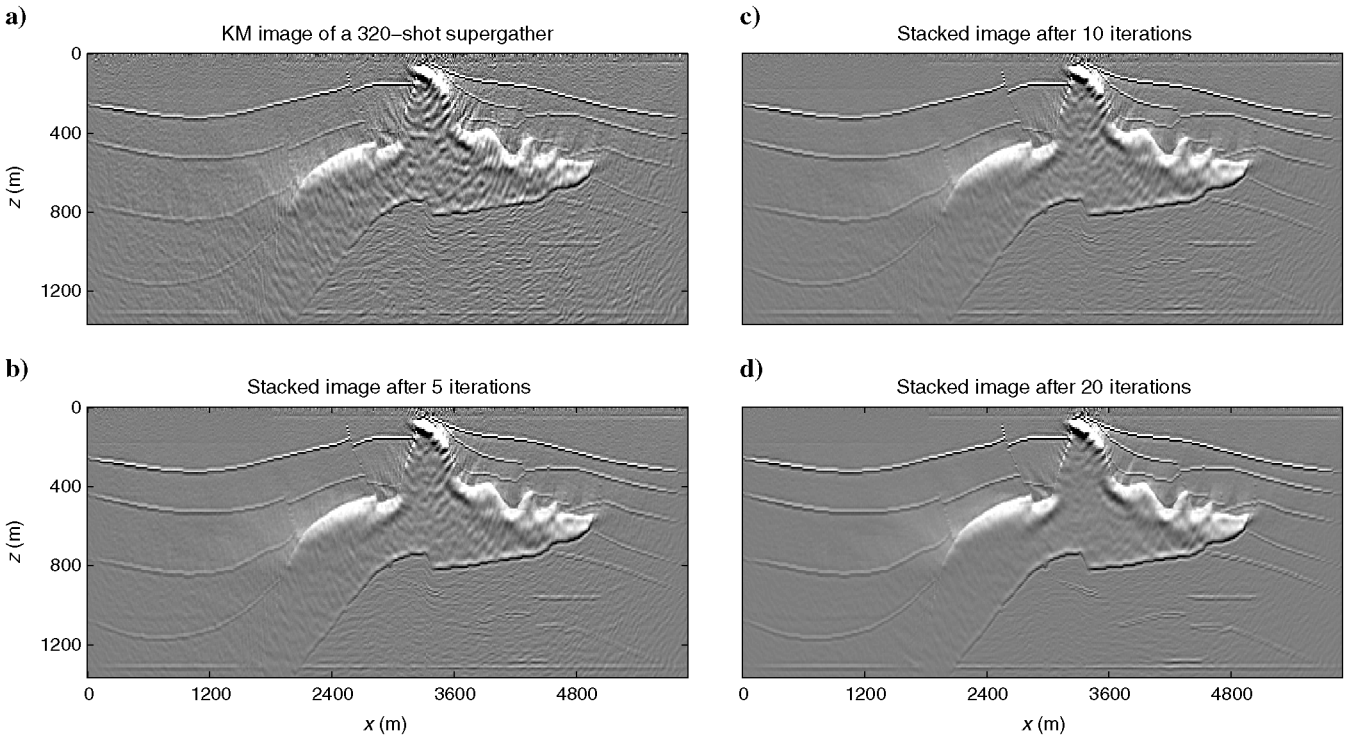

Figure 7. Stacked images for iterative stacking after (a) one iteration; (b) five iterations; (c) 10 iterations; (d) 20 iterations.

enough. To verify this prediction, Figure 9a-9c shows the MLSM images after iteratively migrating a 320-shot supergather; here, the deblurring filter is applied to stabilize and speed up the convergence. It is clear that the image quality increases with the number of iterations. After 60 iterations, the MLSM image is of high quality and mostly free of migration artifacts and crosstalk. It indicates that MLSM can accurately estimate the model even when hundreds of shots are blended together in the processing step, and it does not require too many iterations. Moreover, because the S/N is proportional to $\sqrt{N}$, N being the number of supergathers, the crosstalk noise will be more effectively suppressed when there is more than one supergather.

Dynamic encoding versus static encoding

Following Krebs et al. (2009) and Boonyasiriwat and Schuster (2010), a different time-shift encoding of the shot gathers at each iteration can be used for MLSM; we call this dynamic encoding, compared with static encoding where a shot gather has the same time shift for any iteration. To compare the effectiveness of the dynamic encoding method relative to static encoding, the MLSM of one 320-shot gather is computed with dynamic encoding. Figure 9e and 9f shows the migration images after 10, 30, and 60 iterations. Compared with Figure 9a-9c, the MLSM result is improved, which indicates that dynamic encoding is more effective than static encoding in reducing crosstalk.

To quantitatively show the image quality improvement due to dynamic encoding, the S/N is calculated for the MLSM images and compared with the S/N of the statically encoded images in Figure 10. For each iteration, the corresponding conventional sources LSM image is used as the reference signal. Here, we assume that the convergence rate is the same for conventional sources and multisource LSM. Results clearly show that the dynamic encoding helps suppress the crosstalk and produce images with higher S/N compared to static encoding. With dynamic encoding, the assumption that the crosstalk noise at every iteration is uncorrelated with the crosstalk at previous iterations is closer to the ideal case compared with static encoding. The drawback is that now I supergathers with different encoding functions are required at input, so that the I/O cost will increase and approach that of conventional migration for a large number of iterations (I).

However, our numerical results show that MLSM algorithm is less efficient in reducing crosstalk than the iterative stacking method, as shown in Figure 10. The S/N of the 60-iteration MLSM image with dynamic encoding (Figure 9f) is comparable to the S/N of the 20-fold stacked image (Figure 7d: Note that the migration artifacts in this image are considered as signal in the S/N calculation). One possible explanation is that during the iterations of MLSM the gradients or conjugate directions are computed from different residual data and scaled by different step lengths to make different contributions to the MLSM image and cause the S/N enhancement of MLSM to be suboptimal. Therefore, in real applications, many supergathers (N) should be used. According to equation 11, more supergathers will greatly improve the S/N of final images, which is evident in examining the change from Figure 5f to Figure 5a.

When the processing technique for blending sources is used in full waveform inversion, the S/N of the inverted result is expected to behave in a manner similar to that of MLSM, but analysis is difficult because full waveform inversion is a highly nonlinear process.

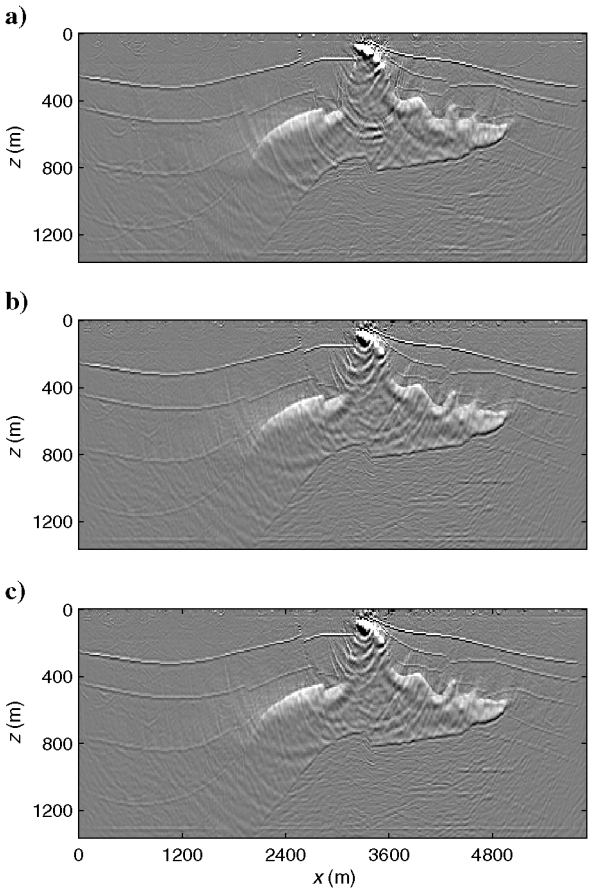

Figure 8. Same as Figure 5, except the supergather clusters consisted of (a) one 40-shot supergather, (b) one 80-shot supergather, and (c) one 160-shot supergather.

Computational cost

Each iteration of iterative LSM costs about two migrations, so the cost of iterative LSM is about $2I$ times that of standard migration. Assuming an ideal land acquisition geometry in which the geophones are fixed and S shot gathers are recorded, the total computational cost in computing the migration image is $\text{cost}^{\text{conv}} \approx S\alpha$ for conventional prestack migration, where α is the cost of one wave-equation migration. In comparison, if N supergathers are migrated, then the cost per iteration of LSM is only $2N\alpha$. This assumes a wave-equation migration method. If I iterations are needed, then the total cost of LSM is $\text{cost}^{\text{multi}} \approx 2N\alpha I$. Therefore, we conclude that the cost of MLSM can be less than standard migration if

$$2NI < S. \tag{13}$$

In our empirical results, a high-quality image is obtained after 60 iterations for a 320-shot supergather, which translates to about 2.7 times speedup if the numerical tests are performed with wave-equation migration or reverse time migration. Meanwhile, the image is free of migration artifacts and with balanced amplitudes (Figure 9c).

Another important saving is the reduction of I/O cost. For Kirchhoff migration, the I/O cost can be the dominant factor for the run time. By statically encoding S shots into a supergather, the I/O cost is reduced to $1/S$ of the original cost, which allows

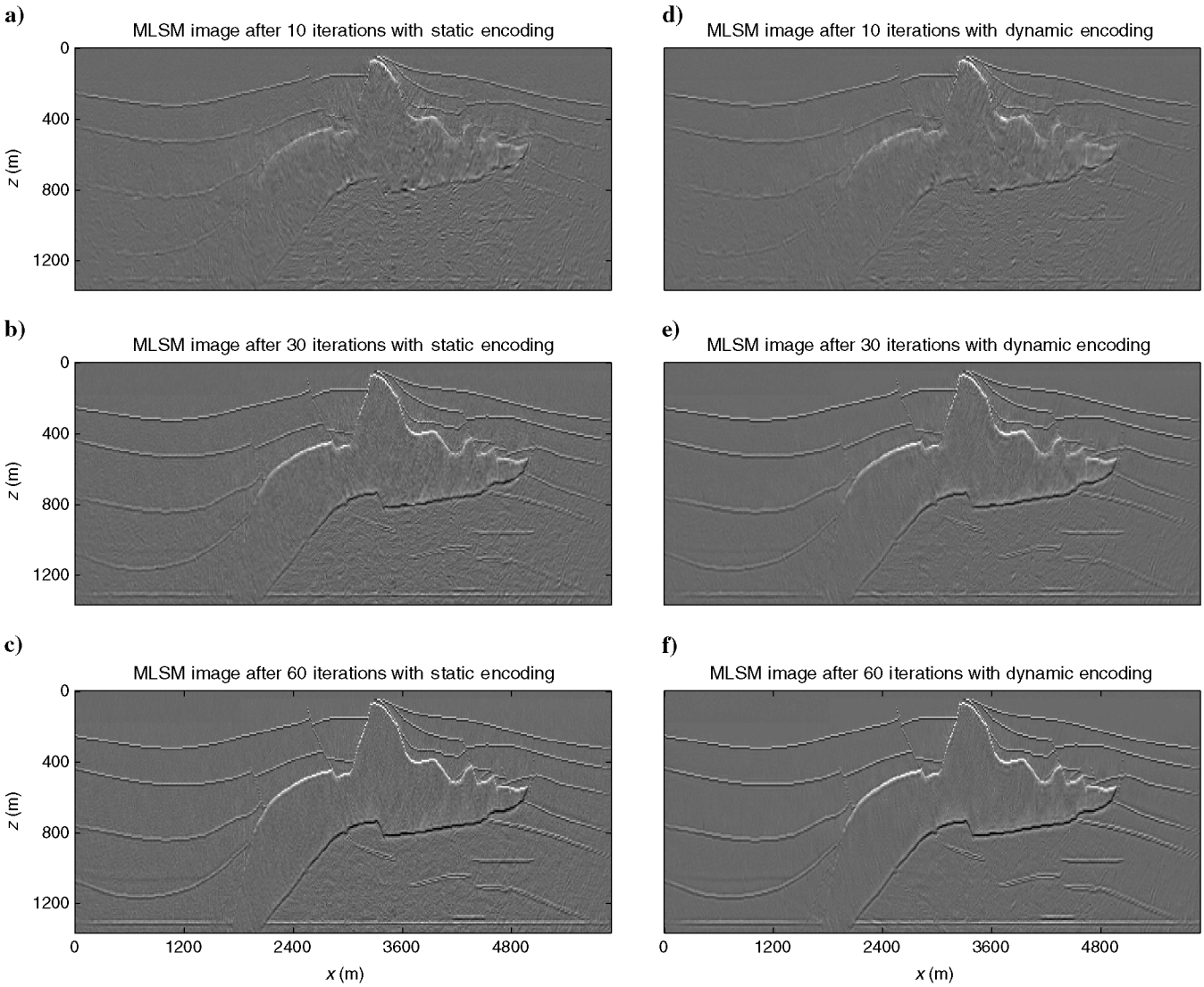

Figure 9. LSM images of a 320-shot supergathers after (a) 10, (b) 30, (c) 60 iterations with static encoding or (d) 10, (e) 30, (f) 60 iterations with dynamic encoding.

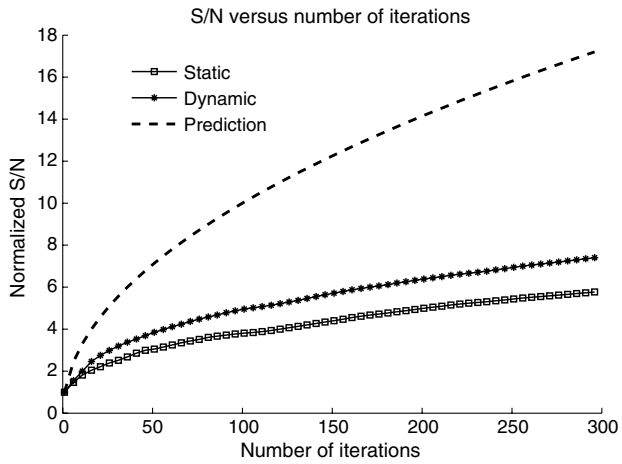

Figure 10. The solid line with squares shows the measured S/N for images of one 320-shot supergather with static encoding; the solid line with stars shows the results with dynamic encoding. Here, the measured S/N is normalized by the first iteration result. The dashed line indicates the prediction from equation 11.

a significant saving in run time of MLSM. For dynamic encoding, if I iterations are needed, I supergathers with different encoding functions are required at input, so that the I/O cost is reduced to I/S of the original cost. Therefore, MLSM with dynamic encoding does not enjoy a large I/O cost reduction if the number of iterations is large. An optional strategy is to periodically stop the iterations in static iterative LSM and restart them at the stopping model but with a new encoding function in the supergathers. In the above calculation, the cost of computation and I/O of preprocessing step is not considered.

CONCLUSION

A MLSM algorithm is proposed to efficiently produce high quality images. This algorithm is implemented with the Kirchhoff migration method and tested with 320 synthetic shot gathers for the 2D SEG/EAGE salt model. An accurate image is obtained by migrating a supergather composite of all these 320 shot gathers after 60 iterations. Compared to conventional Kirchhoff migration image, the I/O cost of MLSM with static encoding is reduced by 320 times. The MLSM image is much more resolved than conventional Kirchhoff migration image because the migration artifacts are suppressed, the reflector amplitudes are balanced, the image resolution is enhanced, and the crosstalk noise is reduced. According to the signal-to-noise ratio analysis, an acceptable number of iterations are needed to achieve high enough S/N. This suggests that high-quality images can be produced with less cost than a conventional migration method, if the MLSM algorithm is implemented with the wave-equation migration method.

Two encoding strategies are discussed in this paper. The MLSM algorithm with static encoding enjoys lower I/O cost compared to the MLSM with dynamic encoding, but our empirical results show that the MLSM with dynamic encoding, on the other hand, is more effective in reducing crosstalk noise introduced by blended sources. Compared with the iterative stacking method, the MLSM algorithm improves the image quality by suppressing the migration artifacts, balancing the reflector amplitudes, and enhancing the image resolution, although the MLSM algorithm requires more iterations to reduce crosstalk than the iterative stacking method. For example, the measured S/N of the 60-iteration MLSM image with dynamic encoding is comparable with the S/N of the 20-fold stacked image.

Future research is needed to address the following questions. First, the MLSM has only been tested with fixed-spread acquisition geometry. The extension to marine acquisition will be significant. Second, the least-square migration seeks a model that optimally fits the data. This process is sensitive to the velocity model, and it is important to reduce this sensitivity for real applications. A third interesting research topic is to look for model-dependent efficient encoding functions.

ACKNOWLEDGMENTS

We are grateful to King Abdullah University of Science and Technology and the sponsors of the 2009 University of Utah Tomography and Modeling/Migration (UTAM) Consortium for their financial support. We also thank the associate editor and three anonymous reviewers for their constructive comments.

APPENDIX A

DEBLURRING FILTER

Following Aoki and Schuster (2009), we use a grid model with an even distribution of isolated point scatterers $\mathbf{m}_{\text{ref}}$ as our reference model. According to equation 6, we get

$$\mathbf{m}_{\text{mig\_ref}} = \mathbf{L}^T\mathbf{L}\mathbf{m}_{\text{ref}} = \mathbf{L}^T\mathbf{d}, \tag{A-1}$$

where $\mathbf{L}$ is the linear diffraction stack operator, which only depends on the background velocity $\mathbf{v}_o$ and the source receiver configurations. Here a column of the $\mathbf{L}^T\mathbf{L}$ matrix represents a migration Green's function (Schuster and Hu, 2000). Then, as shown in Figure A-1, we divide $\mathbf{m}_{\text{ref}}$ into somewhat large subsections centered around each point scatterer. In each subsection, we define a small-sized filter $\mathbf{f}_i$, such that

$$[\mathbf{m}_{\text{mig\_ref}}]_i * \mathbf{f}_i = [\mathbf{m}_{\text{ref}}]_i. \tag{A-2}$$

where i indicates the ith subsection and the notation $[]_i$ denotes the model in the ith subsection. It is very important to choose a proper size for $[\mathbf{m}_{\text{ref}}]_i$ because it has to be big enough to cover the main part of the migration butterflies (Schuster and Hu, 2000). In each

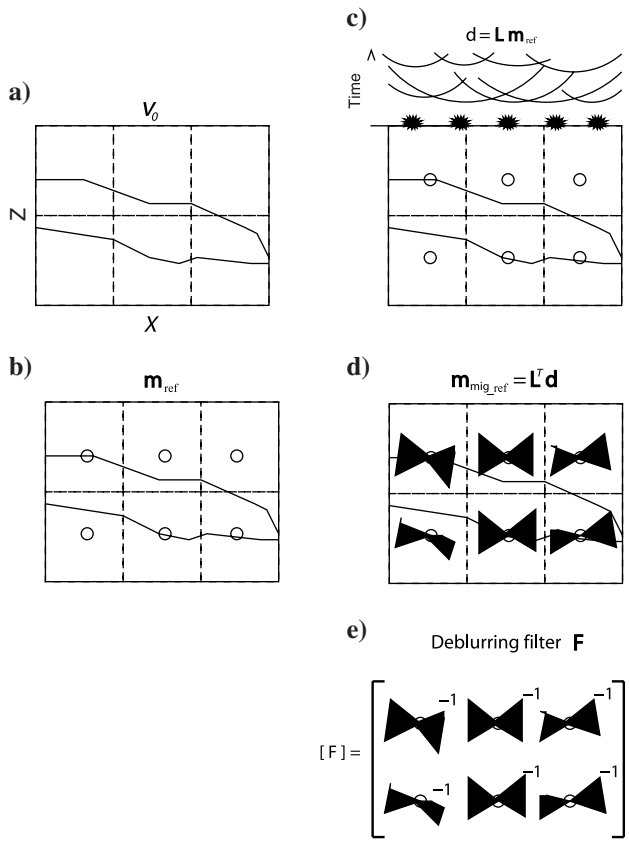

Figure A-1. Steps for computing the deblurring filter. Step (a) define smooth velocity model with point scatterers denoted as circles in (b). Generate multisource data in (c), migrate the multisource data and get an image shown in (d). Step (e), in each subsection, compute a local filter according to $[\mathbf{m}_{\text{mig\_ref}}]_i * \mathbf{f}_i = [\mathbf{m}_{\text{ref}}]_i$ and combine all the local filters into the deblurring filter $\mathbf{F}$.

subsection, the reference model $[\mathbf{m}_{\text{ref}}]_i$ only contains a point scatterer. Thus, $[\mathbf{m}_{\text{migref}}]_i$ represents a migration Green's function, but truncated by the subsection and $\mathbf{f}_i$ is a local filter, which approximates the inverse of the Hessian within the subsection. After solving for $\mathbf{f}_i$ by a least-squares method, we apply $\mathbf{f}_i$ to the ith subsection of the original migration image obtained from the field data, and construct another image $\mathbf{m}_{mf}$. Near the boundaries between subsections, linear interpolation of nearby local filters is computed to make a smoothly varying image. This process can be expressed as

$$\mathbf{m}_{mf} = \mathbf{m}_{\text{mig}} * \mathbf{f}. \tag{A-3}$$

Here, $\mathbf{f}$ represents a bank of stationary filters (each filter is constant within its corresponding subsection). We can rewrite equation A-3 in matrix notation

$$\mathbf{m}_{mf} = \mathbf{F}\mathbf{m}_{\text{mig}}. \tag{A-4}$$

Because $\mathbf{m}_{mf}$ is an approximation of $\mathbf{m}$, and

$$\mathbf{m} = (\mathbf{L}^T\mathbf{L})^{-1}\mathbf{m}_{\text{mig}}, \tag{A-5}$$

then the computed $\mathbf{f}_i$ in each subsection can be formed as the approximated preconditioner matrix:

$$\mathbf{F} \approx (\mathbf{L}^T\mathbf{L})^{-1}. \tag{A-6}$$

We can improve the standard migration image by applying $\mathbf{F}$ to it, or we can use $\mathbf{F}$ as a preconditioner in an iterative LSM solution to speed up convergence.

There are limitations associated with the deblurring filter:

- The subsection needs to be big enough to cover the main part of migration artifacts. It also has to be large to avoid the interface between neighboring sections.
- The migration Green's function is constant within a subsection, so that we can keep the filter constant with the subsection. To honor these two approximations, the velocity model needs to be smooth, so that the variation in the migration Green's function is smooth; hence, we usually use a high-frequency Ricker source wavelet, which makes the migration artifacts smaller.

APPENDIX B

SIGNAL-TO-NOISE RATIO

Consider an observed trace R_t, consisting of a signal trace S_t and zero-mean independent and identically distributed[5] noise n_t of variance σ^2, as in

$$R_t = S_t + n_t, \qquad t = 1, \ldots, T.$$

When M such observed traces are drawn and stacked, we get

$$\begin{aligned}\breve{R}_t &\triangleq \sum_{m=1}^{M} R_t^{(m)} \\ &= \sum_{m=1}^{M}[S_t + n_t^{(m)}] \\ &= MS_t + \sum_{m=1}^{M} n_t^{(m)},\end{aligned} \tag{B-1}$$

where $R_t^{(m)}$ denotes the mth random realization of the signal trace S_t. ($n_t^{(m)}$s are still i.i.d.) The signal and the noise part of the stacked trace $\breve{R}_t$ are denoted by

$$\breve{S}_t \triangleq MS_t \quad \text{and} \tag{B-2}$$

$$\breve{S}_t \triangleq \sum_{m=1}^{M} \breve{n}_t^{(m)}, \tag{B-3}$$

respectively. Note that the root mean squared (rms) amplitude of the stacked signal $\breve{S}_t$ is

$$\begin{aligned}A_M &\triangleq \sqrt{\sum_{t=1}^{T} \breve{S}_t^{\,2}/T} \\ &= M\sqrt{\sum_{t=1}^{T} S_t^{\,2}/T} \\ &= MA_1,\end{aligned} \tag{B-4}$$

where $A_1 = \sqrt{\sum_{t=1}^{T} S_t^2/T}$ is the rms amplitude of the signal trace S_t and the second equality follows from equation B-2; and A_M is defined as the rms amplitude of the M-fold stacked signal $\breve{S}_t$, growing in proportion to M, according to equation B-4. The rms amplitude of the stacked noise $\breve{n}_t$, σ_M, is defined as

$$\begin{aligned}\sigma_M &\triangleq \sqrt{\sum_{t=1}^{T} \langle \breve{n}_t^{\,2} \rangle / T} \\ &= \sqrt{\langle \breve{n}_t^{\,2} \rangle} \\ &= \sqrt{\left\langle \left[\sum_{m=1}^{M} n_t^{(m)} \right]^2 \right\rangle} \\ &= \sqrt{\left\langle \sum_{m=1}^{M} n_t^{(m)2} \right\rangle} \\ &= \sqrt{M}\sigma,\end{aligned} \tag{B-5}$$

where $\langle\rangle$ denotes expectation, the second equality follows because n_ts are identically distributed, the third equality follows from equation B-3, the fourth equality follows because $n_t^{(m)}$s are zero-mean

[5]A sequence of random variables is independent and identically distributed (i.i.d.) if each random variable has the same probability distribution as the others and all are mutually independent.

and independent, and the last equality follows because $n_t^{(m)}$s are identically distributed with variance σ^2. Equation B-5 shows that σ_M grows in proportion to $\sqrt{M}$.

Finally, The S/N of $\breve{R}_t$ is defined as the ratio of rms amplitude of signal over that of noise (Papoulis, 1991),

$$\begin{aligned} \mathrm{S/N} &\triangleq \frac{A_M}{\sigma_M} \\ &= \frac{MA_1}{\sqrt{M}\sigma} \\ &= \sqrt{M}A_1/\sigma, \end{aligned} \tag{B-6}$$

which exhibits a $\sqrt{M}$ enhancement.

REFERENCES

Aoki, N., and G. T. Schuster, 2009, Fast least-squares migration with a deblurring filter: Geophysics, **74**, no. 6, WCA83–WCA93, doi: 10.1190/1.3155162.

Beasley, C. J., 2008, A new look at marine simultaneous sources: The Leading Edge, **27**, 914–917, doi: 10.1190/1.2954033.

Berkhout, A. J. G., 2008, Changing the mindset in seismic data acquisition: The Leading Edge, **27**, 924–938, doi: 10.1190/1.2954035.

Boonyasiriwat, C., and G. T. Schuster, 2010, 3D multisource full-waveform inversions using dynamic random phase encoding: 80th Annual International Meeting, SEG, Expanded Abstracts, 1044, doi: 10.1190/1.3513025.

Claerbout, J. F., 1971, Toward a unified theory of reflector mapping: Geophysics, **36**, 467–481, doi: 10.1190/1.1440185.

Dai, W., and G. T. Schuster, 2009, Least-squares migration of simultaneous sources data with a deblurring filter: 79th Annual International Meeting, SEG, Expanded Abstracts, **28**, 2990–2994.

Dai, W., and G. T. Schuster, 2010, Multi-source wave equation least-squares migration with a deblurring filter: 72nd EAGE Conference & Exhibition, Extended Abstracts, 276–279.

Dai, W., G. Zhan, X. Wang, and G. T. Schuster, 2009, Multi-source least squares migration, waveform inversion, and MVA analysis: Presented at the SEG Invited Workshop Talk.

Duquet, B., K. J. Marfurt, and J. A. Dellinger, 2000, Kirchhoff modeling, inversion for reflectivity, and subsurface illumination: Geophysics, **65**, 1195–1209, doi: 10.1190/1.1444812.

Fromyr, E., G. Cambois, R. Loyd, and J. Kinkead, 2008, FLAM—A simultaneous source wide azimuth test: 78th Annual International Meeting, SEG, Expanded Abstracts, **27**, 2821–2825.

Guitton, A., 2004, Amplitude and kinematic corrections of migrated images for nonunitary imaging operators: Geophysics, **69**, 1017–1024, doi: 10.1190/1.1778244.

Hampson, G., J. Stefani, and F. Herkenhoff, 2008, Acquisition using simultaneous sources: The Leading Edge, **27**, 918–923, doi: 10.1190/1.2954034.

Hu, J., and G. T. Schuster, 2000, Prestack migration deconvolution: 70th Annual International Meeting, SEG, Expanded Abstracts, **19**, 984–987.

Kaplan, S. T., P. S. Routh, and M. D. Sacchi, 2010, Derivation of forward and adjoint operators for least-squares shot-profile split-step migration: Geophysics, **75**, no. 6, S225–S235, doi: 10.1190/1.3506146.

Krebs, J. R., J. E. Anderson, D. Hinkley, R. Neelamani, S. Lee, A. Baumstein, and M.-D. Lacasse, 2009, Fast full-wavefield seismic inversion using encoded sources: Geophysics, **74**, no. 6, WCC177–WCC188, doi: 10.1190/1.3230502.

Kühl, H., and M. D. Sacchi, 2003, Least-squares wave-equation migration for AVP/AVA inversion: Geophysics, **68**, 262–273, doi: 10.1190/1.1543212.

Lynn, W., M. Doyle, K. Larner, and R. Marschall, 1987, Experimental investigation of interference from other seismic crews: Geophysics, **52**, 1501–1524, doi: 10.1190/1.1442268.

Mulder, W. A., and R.-E. Plessix, 2004, A comparison between one-way and two-way wave-equation migration: Geophysics, **69**, 1491–1504, doi: 10.1190/1.1836822.

Nemeth, T., C. Wu, and G. T. Schuster, 1999, Least-squares migration of incomplete reflection data: Geophysics, **64**, 208–221, doi: 10.1190/1.1444517.

Papoulis, A., 1991, Probability, random variables, and stochastic processes: McGraw Hill.

Plessix, R.-E., and W. A. Mulder, 2004, Frequency-domain finite-difference amplitude-preserving migration: Geophysical Journal International, **157**, 975–987, doi: 10.1111/gji.2004.157.issue-3.

Romero, L. A., D. C. Ghiglia, C. C. Ober, and S. A. Morton, 2000, Phase encoding of shot records in prestack migration: Geophysics, **65**, 426–436, doi: 10.1190/1.1444737.

Schuster, G. T., and J. Hu, 2000, Green's function for migration: Continuous recording geometry: Geophysics, **65**, 167–175, doi: 10.1190/1.1444707.

Schuster, G. T., X. Wang, Y. Huang, W. Dai, and C. Boonyasiriwat, 2011, Theory of multisource crosstalk reduction by phase-encoded statics: Geophysical Journal International, **184**, 1289–1303, doi: 10.1111/gji.2011.184.issue-3.

Tikhonov, A., and V. Arsenin, 1977, Solutions of ill-posed problems: V. H. Winston and Sons.

Yu, J., J. Hu, G. T. Schuster, and R. Estill, 2006, Prestack migration deconvolution: Geophysics, **71**, no. 2, S53–S62, doi: 10.1190/1.2187783.

Schuster, G. T., G. Zhan, W. Dai, and C. Boonyasiriwat, 2010, Acoustic multi-source waveform inversion with deblurring: 72nd EAGE Conferenece & Exhibition, Extended Abstracts, G002.